Mustansiriyah Journal of Pure and Applied Sciences

www.MJPAS.com

A Comparative Study of Structural and Optical Properties of Al-Doped Fe_2O_3 Films: Experimental and DFT Approach

K.A. Mishjil[1], N.H. Numan[2], M.S. Othman[3a,b], N.F. Habubi[4], N.N. Jandow[1] and H.G. Rashid[1]

[1]Department of Physics, College of Education, Mustansiriyah University, Iraq.

[2]Laser and optoelectronic engineering department, University of Technology-Iraq

[3a]Faculty of Education, Soran University, Soran 44008, Erbil, Kurdistan Region, Iraq.

[3b]Scientific Research Center, Soran University, Kurdistan Region, Iraq.

[4] Department of Radiation and Sonar Technologies, Alnukhba University College

[4] n.fadhil@alnukhba.edu.iq

A B S T R A C T

Thin films of undoped iron oxide and aluminium-doped Fe_2O_3, with 1%, 2%, and 3% Al content, were deposited using a spray pyrolysis technique. X-ray diffraction (XRD) and UV-VIS spectroscopy were used to examine the structural and optical characteristics of the deposited films. According to the findings and the density functional theory (DFT), Fe_2O_3 has a cubic structure. DFT suggested the exchange-correlation functions via the generalized gradient approximation (GGA). Transmittance decreased from 61% (for Fe_2O_3) to 41% (for Al-doped with 3%). According to experimental optical measurements, the energy gap increased from 2.27 eV to 2.65 eV. However, in theoretical results, with an increase in Al doping, it grew from 2.17 eV to 2.45 eV. Theoretical predictions and experimental data were highly compatible..

Keywords: *Iron oxide film, Aluminum, Structural, Optical, DFT*

1. Introduction

Metal oxide photocatalysts, in particular, have shown exceptional performance in energy-related applications, such as photocatalytic destruction of natural compounds with absorption wavelengths that extend into the visible region [1–6]. Fe_2O_3 is a remarkable oxide material with a 2.2 eV optical bandgap that absorbs visible light and gathers up to 46% of solar spectrum energy. In addition, the Fe_2O_3 solid sphere has increased photocatalytic activity for rhodamine breakdown in visible light [7]. It also offers appealing features, such as a unique magnetic structure and a highly coupled electronic nature [8, 9]. Another study used (DFT) simulations to investigate the charge distribution at the water/Fe_2O_3 interface in their work for properties of Fe_2O_3. Both theory calculations and experiments with aluminium-doped-Fe_2O_3 photoelectrodes were performed.[10]. Fe_2O_3 thin films have been described optically and electrically [11,12]. Various physical techniques, such as magnetron sputtering [13], have been synthesized for these films due to their great catalytic activity, ubiquitous availability, and environmental protection. Chemical methods such as

thermochemical synthesis[14], chemical vapor deposition [15], and the sol-gel procedure [16] have also been used. Since it was the first time Spray Pyrolysis Technique and DFT were employed to evaluate the structural and optical characteristics of Fe_2O_3 films with doped aluminium, the study was necessary for investigation.

2. Experimental and Method of Calculation

a) Experimental

A glass atomizer manufactured in the lab with a one mm output nozzle was utilized for the experiment to perform spray pyrolysis. After many trials to get an acceptable homogeneity, the films were grown at an optimum glass substrate temperature of 450 °C. At this temperature, the smoothest films were produced. A uniform mixture of the aqueous solution was created by combining 0.1M of ($AlCl_3$), as a source of Al, with (1-3 wt%). Using a magnetic stirrer, 0.1M ($FeCl_3.6H_2O$), as a source of Fe in 100 mL of deionized water. The most efficient setting was spray time (5 second), which was stopped by 2 minutes to prevent overcooling and deposition rate (8 ml/min). The distance between spout and base was fixed (30 ±1 cm), and the carrier gas (filtered compressed air) pressure of 5bar. Using the StellarNet TF method, the samples' thickness was calculated and found to be around (400± 30 nm). The transmittance and absorbance under investigation were measured utilizing UV- Visible spectrophotometer (Shimadzu Company Japan).

b) Modeling

By employing the plane-wave pseudopotential approach, density functional calculations are done for each structure to examine the structure and optical characteristics of the Al-doped Fe_2O_3 and Fe_2O_3 films. Generalized gradient approximation (GGA) was recommended by Perdew, Burke, and Ernzerhof (PBE) [17,18]. All varieties of Fe_2O_3 films were prepared and optimized using the CASTEP module of Material Studio with periodic boundary settings [19]. Ultrasoft pseudopotentials were created to simulate the interaction between ions and valence electrons. [20] The cutoff energy of 440 eV was selected for the plane-wave basis. The geometry optimization convergence condition is shown in Table 1. The same characteristics of all films, like reflection and absorption, are investigated by Maxwell's equations (M.E.). A nanomaterial was utilized to test the optical response to electromagnetic (E.M.) radiation.

Table 1. The convergence parameters for geometry optimization.

Fe_2O_3 films	Monkhorst-Pack Grids	Maximum Force, MF $(eV/Å) \times 10^{-2}$	Maximum Stress, MS (GPa) $\times 10^{-4}$	Maximum Displacement, MD (Å) $\times 10^{-4}$	Energy, E $(eV/atom) \times 10^{-5}$	Lattice Parameters (nm)
Pure	4×4×5	5	10	20	2	80.15
Al: Fe_2O_3 (0.25)	3×3×4	1	2	5	0.5	79.53
Al: Fe_2O_3 (0.50)	4×3×6	1	2	5	5	78.98
Al: Fe_2O_3 (0.75)	3×2×6	1	2	5	0.5	77.37

3. **Results and Discussions**

Both optical absorption and optical band-disallowed energy have been considered. At equilibrium, the structural parameters of compounds were calculated in the same way as the first step: minimizing the crystal's lattice parameter, which is the ratio of total energy to volume. Figure 1 shows the structures of Iron oxide with Al-doped as a function of $Al_x(Fe_{1-x})_2O_3$ compounds at x concentrations, where x = 0, 0.25, 0.5, and 0.75, respectively.

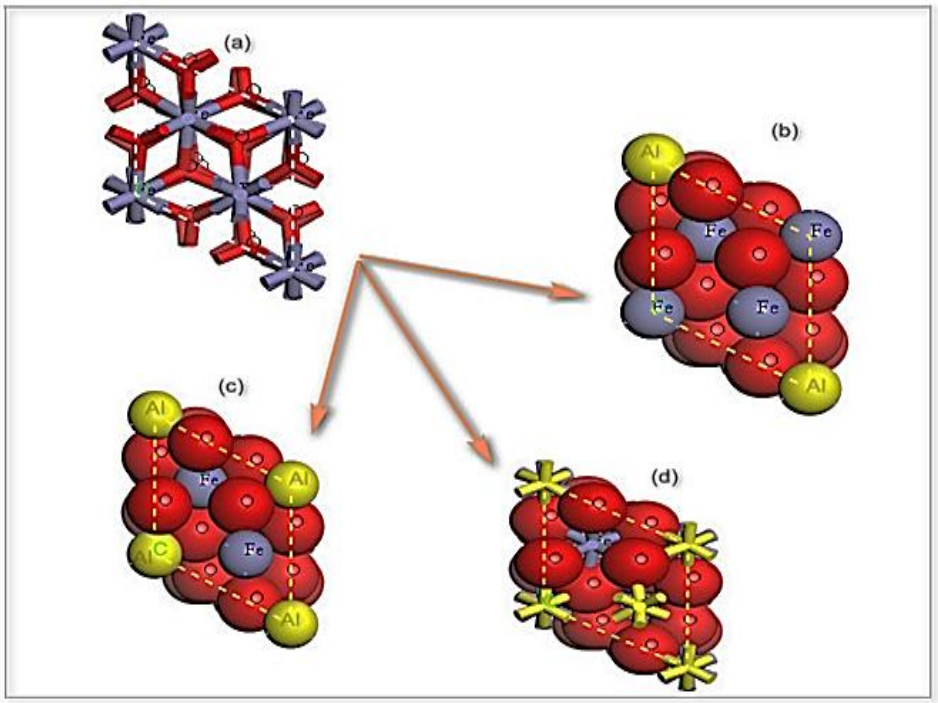

Figure 1. The structures of Iron oxide with Al-doped.

XRD patterns of Fe_2O_3:Al thin films are shown in Figure 2. The creation of the rhombohedral crystal structure of the Fe_2O_3 phase is indicated by the existence of diffraction peaks correlating to (104), (110), (024), and (116) planes according to (JCPDS card no. 33-0664), which are in good agreement with results obtained by Lassoued *et. al.* [21] There was no evidence of aluminium or aluminium oxide. It was found that raising the Al content by up to 3% caused the intensity of (104) peak to rise initially. It is also important to note that although (104) is still the favoured orientation, once Al atoms were added, a tendency for crystallites to grow along (110) plane occurred. Peak positions did, however, shift to somewhat higher angles. The lesser Al^{3+} (0.53) ionic radius than Fe^{3+} (0.69) causes a shift in peak positions to higher angles. Al atoms occupy the Fe sites efficiently, according to the XRD pure phase, resulting in a 2θ shift . This behavior agrees with El-Shater et al. [22].Utilizing DFT simulation to determine the energy band structures for Fe_2O_3 and Al-doped Fe_2O_3 films after all types of films have been optimized using the input values stated in Table (1).

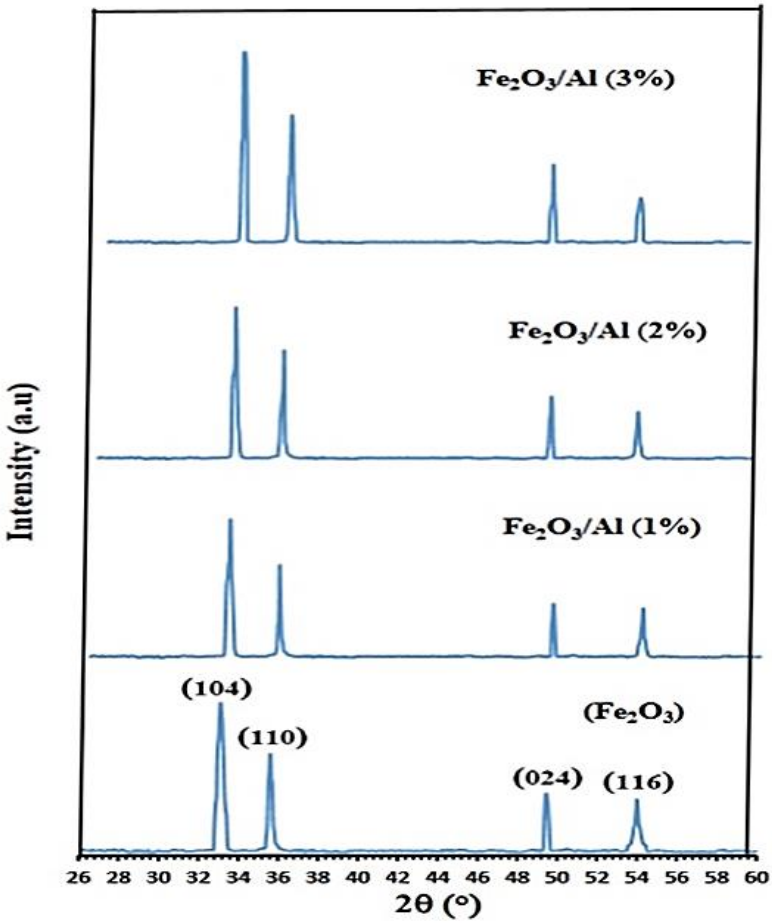

Figure 2. XRD patterns of the intended films

By using Al_x $(Fe_{1-x})_2O_3$ compounds at x concentrations (x = 0, 0.25, 0.5, and 0.75, respectively). Doping aluminium differently affects the energy band structure. For many electronic applications, these properties are exceptional and crucial. Scherrer's formula in equation 1, which considers the width of the x-ray diffraction line, was employed to calculate the average grain size (D) [23].

$$D = \frac{0.9\lambda}{\beta cos\theta} \quad (1)$$

Where β is (FWHM in radians), θ is Bragg's angle, and λ is the wavelength of x-rays. The crystallite size of Fe_2O_3 was 18 nm, but the D values of Al-doped Fe_2O_3 range was between 21 to 26 nm as the Al concentration rose.

The following relationships could be used to illustrate Warren-Scherrer's correction method for calculating average grain size.

$\beta_o = \beta_s - \beta_i$ (Lorentzian distribution)

$\beta_o^2 = \beta_s^2 - \beta_i^2$ (Gaussian distribution)

The Dislocation density (δ) and microstrain (ε) of intended films were evaluated by equations 2 and 3 [24]:

$$\varepsilon = \frac{\beta cos\theta}{4} \quad (2)$$

$$\delta = \frac{1}{D^2} \quad (3)$$

As seen in Table 2, the lattice strain decreases as the Al content rises. Contrarily, Fe_2O_3 thin films have a higher lattice strain than doped films, and the microstrain was reduced by Al incorporation. The average microstrain of Al-doped Fe_2O_3 at 3% decreased from 1.89×10^{-3} for Fe_2O_3 to 1.34×10^{-3}. The dislocation density displays the exact microstrain property.

Table 2. Structural parameters of the intended films.

Sample	Crystallite size (nm)	Lorentzian distribution (nm)	Gaussian distribution (nm)	Dislocation density x 10^{15}(line/m^2)	Microstrain x10^{-3}
Pure Fe_2O_3	18	22	23	3.08	1.89
1% Al-doped Fe_2O_3	21	28	29	2.26	1.67
2% Al-doped Fe_2O_3	22	30	31	2.06	1.59
3% Al-doped Fe_2O_3	26	38	41	1.47	1.34

Figure 3 shows the absorbance of the intended films (Exp.). The absorbance for doped films increased dramatically at wavelengths less than 500 nm. Ayed agrees well with the behavior of improving the grain size[25].

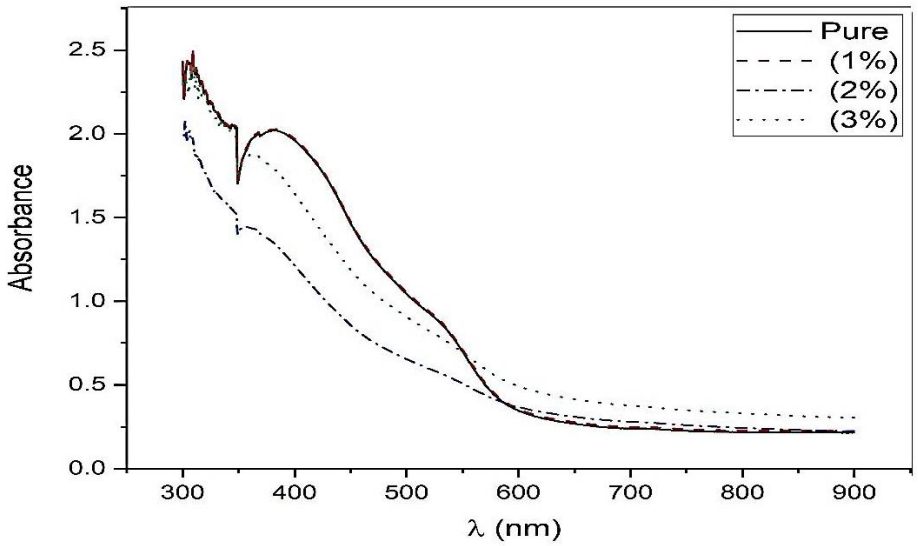

Figure 3..Absorbance (experimental) of the deposited films

Additionally, doping can be increased to change and improve the energy band gap values. Our findings demonstrate that increasing doping will increase the energy levels of the valence and conduction band, as shown in Figure 4. According to underestimating the bandgap, obtaining a correct optical bandgap is challenging. Our calculations used an energy scissor operator with 0.87 eV to fit the absorption edge to the observed result. This theoretical method works for many systems [26-28]. The starting absorption values at the beginning are 2.17, 2.23, 2.37 and 2.49 eV, respectively. These formations have semiconductor properties due to the growing valence and conduction band gaps caused by Al doping in all samples. Through the Kramers-Kronig [29], the absorbance spectrum dependence is tightly connected.

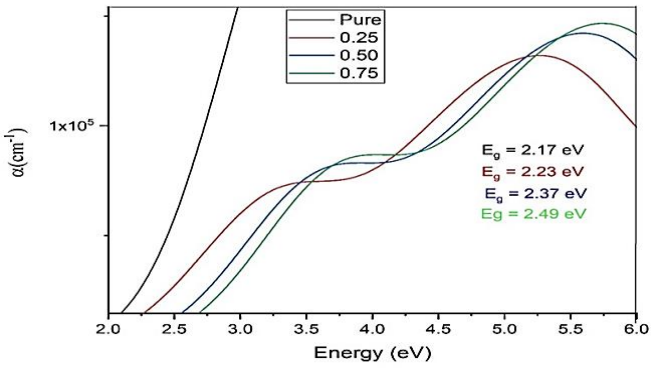

Figure 4. The optical band gap energy of $Al_x (Fe_2)_{1-x}O_3$

The experimental transmittance spectra of Fe_2O_3 and Fe_2O_3 with Al doping are shown in Figure 5. In the observed data, the transmittance was 61% for the undoped film. Still, it decreases with Al concentrations as 1%, 2% and 3%, respectively, for 58%, 46% and 42%, in the visible and near-infrared area (450–900 nm). Crystal flaws' enhanced photon scattering.

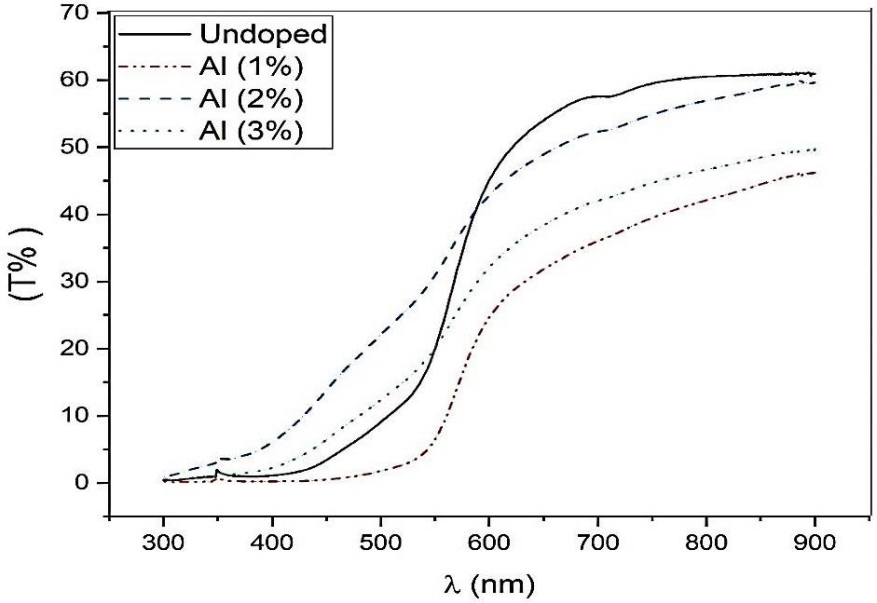

Figure 5. Transmittance (experimental) of the deposited films

The energy bandgap E_g is obtained by Tauc's relation, as shown in equation 4[30].

$$(\alpha h\nu) = A\left(h\nu - E_g\right)^n \quad (4)$$

Where n equals ½ for direct transition, A is a constant, $h\nu$ is photon energy, and Figure 6 shows the direct transition. Optical bandgap (E_g) was determined from the plots of $(\alpha h\nu)^2$ vs. $h\nu$ of the deposited films. The Fe_2O_3 thin film value was 2.27 eV, which agrees with the reported values [29]. For 1 %, 2% and 3% Al doping, the direct bandgap value of the films was (2.5, 2.6 and 2.65) eV. So, Al doping affects the bandgap value of Fe_2O_3 thin films.

Figure 7 (a and b) demonstrates the increase of the experimentally and theoretically calculated energy gap with increased Al content, verifying that the conduction band edge increases with doping concentration. This result agrees with the references [30,31].

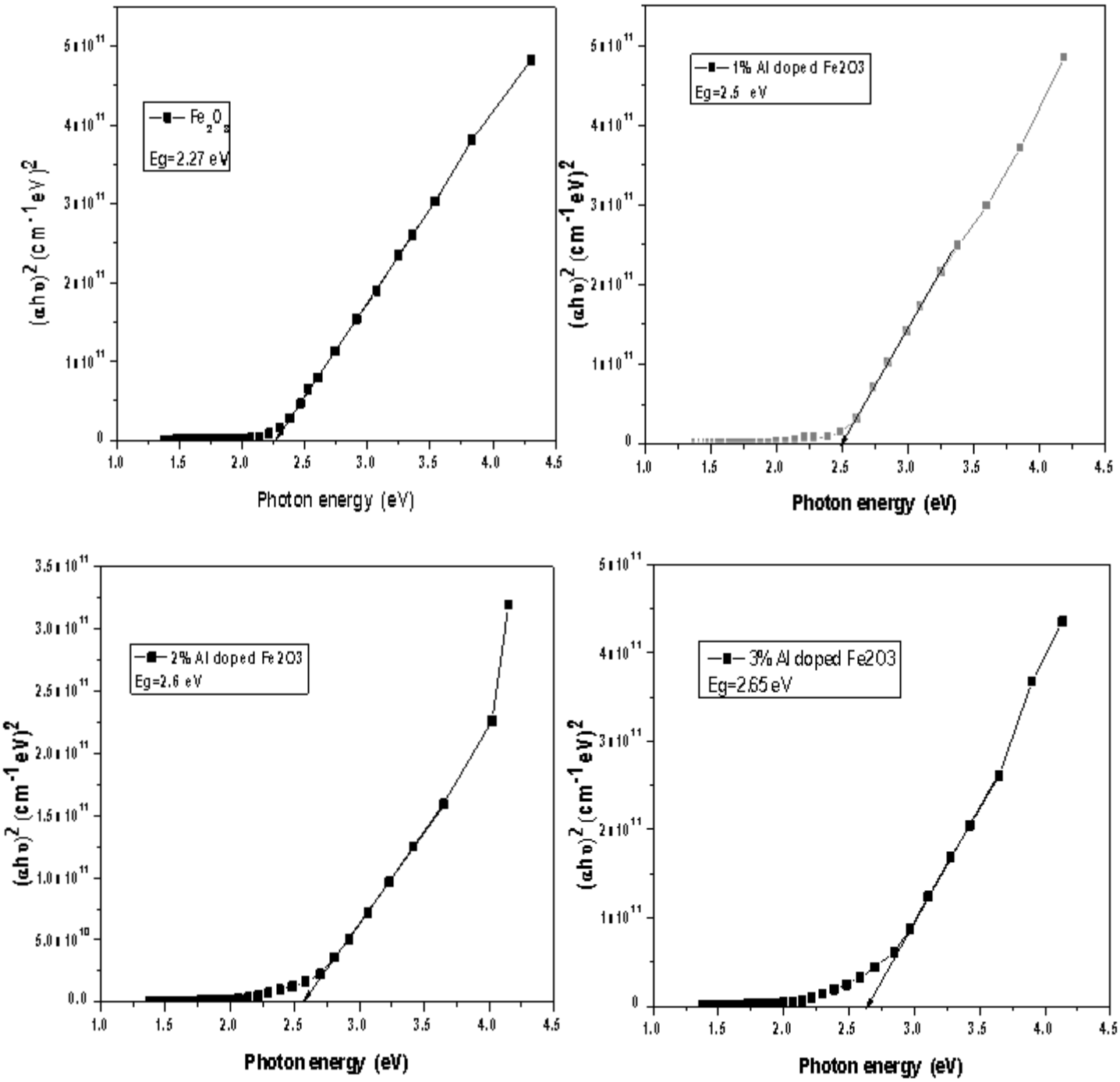

Figure 6. Experimental results via photon energy $(\alpha h\nu)^3$ *vs.* $(h\nu)^2$ for the grown films**.**

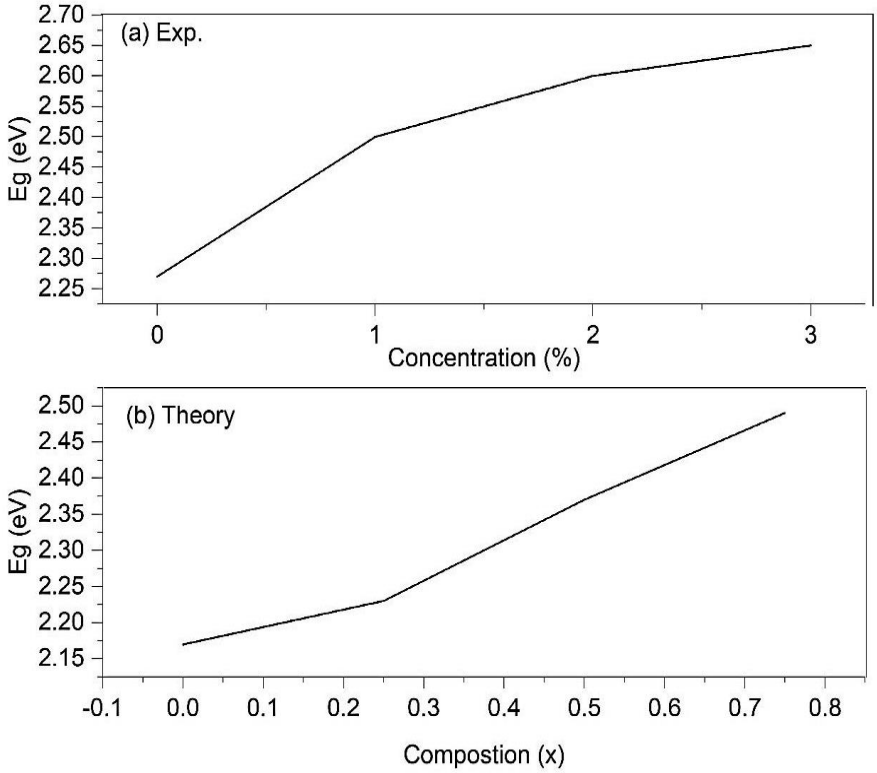

Figure 7 (**a**, **b).** Increase in the determined optical bandgap energies experimentally and theoretically via increasing Al content.

4.Conclusions

On glass substrates, thin films of pure Fe_2O_3 and Fe_2O_3 doped with Aluminum (Al: Fe_2O_3) at 1%, 2%, and 3% concentrations were produced by spray pyrolysis. The cubic structure of Fe_2O_3 was demonstrated using XRDand DFT results. DFT provided the exchange-correlation functions using (GGA). Optical experiments revealed that doping decreased transmittance from 61% to 42%. Similarly, the optical energy gap was increased from 2.27 eV to 2.65 eV even though theoretical results indicated a decrease with increasing Al doping concentration, from 2.17 eV to 2.49 eV. Theoretical predictions and experimental data were very compatible. Electronic devices rely mainly on the resulting optical properties. The results also revealed that the research was fascinating and immediately applicable to electronic and technical applications. These qualities imply that Al-doped Fe_2O_3 can be employed in photoelectron device applications.

Acknowledgement
The researchers acknowledge the assistance of Mustansiriyah University and Alnukhba University College.

References

[1] Tian, C. M., Li, W. W., Lin, Y. M., Yang, Z. Z., Wang, L., Du, Y. G., ... & Zhang, K. H. (2020). Electronic structure, optical properties, and photoelectrochemical activity of sn-doped fe2o3 thin films. *The Journal of Physical Chemistry C*, *124*(23), 12548-12558.

[2] Rzaij, J. M., & Habubi, N. F. (2022). Enhancing the CO2 sensor response of nickel oxide-doped tin dioxide thin films synthesized by SILAR method. *Journal of Materials Science: Materials in Electronics*, *33*(15), 11851-11863.

[3] Othman, M. S., Mishjil, K. A., Rashid, H. G., Chiad, S. S., Habubi, N. F., & Al-Baidhany, I. A. (2020). Comparison of the structure, electronic, and optical behaviors of tin-doped CdO alloys and thin films. *Journal of Materials Science: Materials in Electronics*, *31*, 9037-9043.

[4] Hu, Y. S., Kleiman-Shwarsctein, A., Forman, A. J., Hazen, D., Park, J. N., & McFarland, E. W. (2008). Pt-doped α-Fe2O3 thin films active for photoelectrochemical water splitting. *Chemistry of Materials*, *20*(12), 3803-3805.

[5] Droubay, T., Rosso, K. M., Heald, S. M., Mccready, D. E., Wang, C. M., & Chambers, S. A. (2007). Structure, magnetism, and conductivity in epitaxial Ti-doped α− Fe 2 O 3 hematite: Experiment and density functional theory calculations. *Physical Review B*, *75*(10), 104412.

[6] Ruvalcaba-Manzo, S. G., Castillo, S. J., Flores-Acosta, M., Ochoa-Landín, R., & Ramírez-Bon, R. (2022). Study of optical, morphological, structural, and chemical properties of CdO thin films synthesized by thermal annealing transformation of CdCO3 thin films. *Optical Materials*, *132*, 112742.

[7] Liu, G., Deng, Q., Wang, H., Ng, D. H., Kong, M., Cai, W., & Wang, G. (2012). Micro/nanostructured α-Fe 2 O 3 spheres: synthesis, characterization, and structurally enhanced visible-light photocatalytic activity. *Journal of Materials Chemistry*, *22*(19), 9704-9713..

[8] Lassoued, A., Lassoued, M. S., Dkhil, B., Ammar, S., & Gadri, A. (2018). Synthesis, photoluminescence and Magnetic properties of iron oxide (α-Fe2O3) nanoparticles through precipitation or hydrothermal methods. *Physica E: Low-dimensional Systems and Nanostructures*, *101*, 212-219.

[9] Jiao, F., Harrison, A., Jumas, J. C., Chadwick, A. V., Kockelmann, W., & Bruce, P. G. (2006). Ordered mesoporous Fe2O3 with crystalline walls. *Journal of the American Chemical Society*, *128*(16), 5468-5474..